SUPPLEMENTAL INFORMATION

Ubiquitous antigen-specific T-regulatory type 1 cells variably suppress hepatic and extra-hepatic autoimmunity

Channakeshava Sokke Umeshappa[1], Jacques Mbongue[1], Santiswarup Singha[1], Saswat Mohapatra[1], Jun Yamanouchi[1], Justin A. Lee[1], Roopa Hebbandi Nanjundappa[1], Kun Shao[1], Urs Christen[2], Yang Yang[1,3], Kristofor K. Ellestad[1], and Pere Santamaria[1,4*]

Supplemental Materials and Methods

Mice

NOD/LtJ and C57BL/6 mice were purchased from the Jackson Laboratory (Bar Harbor, ME). 8.3-NOD.*G6pc2*$^{-/-}$.*Tcra*$^{-/-}$ were produced in our laboratory (1). NOD.*c3c4* mice, were obtained from Jackson Laboratory and bred in our animal facility. RIP-DTR.NOD transgenic mice were generated by backcrossing an X-chromosome-linked rat-insulin promoter-driven human diphtheria toxin receptor (RIP-DTR) transgene from transgenic B6 mice (a gift from P. Herrera) (2) into the NOD background for more than 10 generations. All the studies described here were approved by the institutional animal care committee of the Cumming School of Medicine at the University of Calgary.

Antibodies, flow cytometry

Anti-murine LAG-3 (C9B7W) and Anti-latent-TGF-β (LAP) (TW7-16B4) mAbs were obtained from eBioscience (San Diego, CA) and BioLegend (San Diego, CA), respectively. FITC-, PE-, APC-, BV780- or PerCP-conjugated mAbs against mouse CD4 (RM4-5), CD8 (53-6.7), B220 (RA36B2) and CD49b (HMα2) were purchased from BD Biosciences (San Diego, CA). PE-conjugated pMHC class II tetramers were produced using biotinylated pMHC monomers. pMHC class II tetramer staining and phenotypic marker analysis were done as described (3) with minor modifications. Briefly, after avidin incubation (15 min at RT), blood leukocytes, and single cell suspensions from spleen, lymph node, liver mononuclear cells, and bone marrow cells were stained first with pMHC tetramer (5μg ml^{-1}) in FACS buffer (0.05% sodium azide and 1% FBS in PBS) for 60 (all tetramers except MOG_{38-49}/IA^b) or 120 min (for MOG_{38-49}/IA^b) at 37°C, and later with FITC-conjugated anti-mouse CD4 (5μg ml^{-1}) and PerCP-conjugated anti-mouse B220 (2μg ml^{-1}; as a 'dump' channel) for 30 min at 4 °C. After washing, cells were fixed (1% paraformaldehyde in PBS) and analyzed with FACScan, FACSaria, or BD LSRII flow

cytometers. For phenotypic analyses, the cells were incubated with anti-FcR Abs, and then stained with cell surface marker antibodies diluted 1:100 in FACS buffer (at 4°C for anti-CD49b and anti-LAP Abs, and at 37°C for anti-LAG-3 Abs) followed by pMHC tetramer, FITC-conjugated anti-mouse CD4 (5μg ml^{-1}) and PerCP-conjugated anti-mouse B220. Upon staining, cells were washed, fixed, and analyzed by FACS. FlowJo software was used for analyses.

Adenovirus

Replication-deficient adenoviruses expressing human CYP2D6 (Ad-2D6) or formiminotransferase cyclodeaminase (Ad-hFTCD) (target autoantigens in human AIH) were generated as described (4, 5). The viruses were amplified in Ad-293 T cells and purified using Adeno-X Maxi Purification Kit (Clontech). The viral titer was measured using the End-point Dilution Assay or Adeno-X Rapid Titer Kit (Clontech).

pMHC monomers and peptides

Recombinant pMHC class II monomers were purified from supernatants of CHO-S cells transduced with lentiviruses encoding a monocistronic message in which the peptide-MHCα and MHCβ chains of the complex were separated by the ribosome skipping P2A sequence, or with lentiviruses encoding a peptide-tethered MHCβ chain or the MHCα chain. The peptide was tethered to the amino terminal end of the MHCβ chain via a flexible GS linker and the MHCα chains were engineered to encode a BirA site, a 6xHis tag, a twin strep-tag and a free Cys at their carboxyterminal end. The secreted, self-assembled pMHC class II complexes were purified by sequential nickel and Strep-Tactin® chromatography and used for coating onto NPs or processed for biotinylation and tetramer formation. The epitopes encoded in the murine monomeric constructs were selected based on predicted MHCII-binding capacity using RANKPEP (http://imed.med.ucm.es/cgi-bin/rankpep_mif.cgi) and/or GPS-MBA (http://mba.biocuckoo.org/).

Flagellin$_{462-472}$ is a sequence derived from the conserved amino-terminal domain of flagellin (a shorter version of CBir1$_{456-475}$ peptide described by Cong et al. (6)). The sequences of the different epitopes are: PDC-E2$_{166-181}$/IA^{g7} (LAEIETDKATIGFEVQ), CYPD2D6$_{398-412}$/IA^{g7} (LITNLSSALKDETVW), BDC2.5mi/IA^{g7} (AHHPIWARMDA), MOG$_{36-50}$/IA^{g7} (EVGWYRSPFSRVVHL), Fla$_{462-472}$/IA^{b} (VKYSNANILSQ), MOG$_{38-49}$/IA^{b} (GWYRSPFSRVVH), PDC$_{94-108}$/IA^{b} (TLDLAAAAAPQAAPA) and CYPD2D6$_{353-367}$/IA^{b} (QARMPYTNAVIHEVQ). Synthetic mMOG$_{36–55}$ (EVGWYRSPFSRVVHLYRNGK) peptide was purchased from Genscript (Piscataway, NJ). The amino acid residue numbers for each peptide correspond to those found in the mature form of the corresponding antigens.

Nanoparticles, pMHCII-NP synthesis, and purification

Nanomedicines were synthesized by coating pMHCs onto pegylated iron oxide NPs (PFM-NPs) as described (7) Briefly, PFM-NPs were produced by thermal decomposition of Fe(acac)$_3$ in the presence of 2 kDa methoxy-PEG-maleimide. The NPs were purified using magnetic (MACS) columns (Miltenyi Biotec, Auburn, CA). Free Cysteines (controls) or pMHCs, carrying a free carboxyterminal Cys, were conjugated to the maleimide-functionalized PFMs in 40mM phosphate buffer, pH 6.0, containing 2mM EDTA, 150mM NaCl overnight at room temperature. The pMHC-conjugated NPs were separated from free pMHC using magnetic columns, sterilized by filtration through 0.2μm filters and stored in water or PBS at 4^{o}C. Quality control was done using transmission electron microscopy, dynamic light scattering, and native and denaturing gel electrophoresis. pMHC content was measured using Bradford assay (Thermo Fisher Scientific) and SDS-PAGE.

pMHCII-NP therapy in NOD/Ltj mice

Cohorts of 10-wk old prediabetic female NOD/ShiLtJ mice were treated with 20 μg of pMHCII-NPs (pMHC weight) or Cys-NPs (the exact same amount of iron given with the pMHC-coated NPs) i.v. twice weekly for 5 wk.

Diphtheria toxin treatment in RIP-DTR.NOD mice

Female 10-wk old RIP-DTR-transgenic NOD mice were given 400 ng of DT intraperitoneally to kill 50% of the beta cells that express DTR. Both DT-treated and untreated mice were treated with 10 doses of $PDC_{166\text{-}181}/IA^{g7}$-NPs or $CYPD_{398\text{-}412}/IA^{g7}$-NPs (twice weekly i.v. for 5 weeks).

pMHCII-NP therapy for EAE in NOD and C57BL/6 mice

Female 8-10 wk-old NOD mice were immunized with 250 μg of $pMOG_{36-55}$ in CFA s.c. on either side of the flank region above the base of the tail under isofluorane anesthesia as described (3). The mice received 350 ng of Pertussis toxin i.v. on days 0 and 2 relative to peptide immunization. Mice were weighed and scored on day 0 and then daily starting on day 14 after immunization, and scores were plotted on a 5-point scale (3). Since these mice develop an asynchronous relapsing-remitting form of EAE, all the mice which developed signs of EAE during the first 25 days were randomized into treatment with Cys-NPs or pMHCII-NPs on days 32 or 41 after immunization. All mice were treated twice a week for 9 wk. Histopathological lesions in the cerebellum of treated mice were scored based on the degree of inflammation and demyelination.

Female 8 wk-old C57BL/6 mice were immunized with 200 μg of $pMOG_{36-55}$ in CFA s.c. and received 300 ng of Pertussis toxin i.v. on days 0 and 3 relative to peptide immunization. Since these mice develop a synchronous non-remitting form of chronic EAE, all the mice were randomized into treatment when they reached a score of 1.5. Clinical and histopathological scoring for EAE was done as described above.

pMHCII-NP therapy for AIH in C57BL/6 and NOD mice

AIH was induced by infecting 6 wk-old female C57BL/6 mice with an adenovirus encoding human CYP2D6 (Ad-hCYPD, $3x10^8$ plaque forming units (PFU) i.v. and i.p. per mouse) as described (4). To induce AIH in NOD mice, $1x10^{10}$ PFU of a replication-defective adenovirus encoding human formiminotransferase cyclodeaminase (Ad-hFTCD) (a target autoantigen in AIH Type 2) was injected i.v. as described (5). Four-to-six weeks later, cohorts of mice with established AIH were treated with 20 μg of pMHCII-NP s or Cys-NPs i.v. twice weekly for 5-6 wk. Histopathological scoring was done using the Ishak scale (8, 9), which evaluates both fibrosis (0-6) as well as necroinflammatory sequelae, including interface hepatitis (0-4), confluent necrosis (0-6), lobular inflammation (0-4) and portal inflammation (0-4).

pMHCII-NP therapy for superimposed EAE and AIH in C57BL/6 mice

AIH was induced in 6 wk-old female C57BL/6 mice as described above. Four weeks later, mice were immunized to induce EAE, also as described above. All the EAE mice were randomized into treatment when they reached a score of 1.5. Cohorts of mice with established AIH and EAE were treated with 20 μg of pMHCII-NPs s or Cys-NPs twice weekly i.v. for 5 consecutive weeks. The effects of treatment on AIH and EAE were determined as described above.

To ascertain whether treatment of AIH with pMHCII-NP prior to inducing EAE was able to release cognate ubiquitous antigen-specific TR1 cells to blunt EAE, cohorts of mice with established AIH were first treated with pMHCII-NPs or Cys-NPs twice weekly i.v. for 5 consecutive wk as shown in **Supplementary Fig. 4.** The treated mice were then immunized to induce EAE, as described above. All the EAE mice in pMHCII-NP- and Cys-NP-pre-EAE treatment groups were randomized into different treatment groups and treated with 20 μg of pMHCII-NPs or Cys-NPs twice weekly i.v. for 5-6 additional weeks. The effects of treatment on AIH and EAE were determined as described above.

pMHCII-NP therapy for superimposed EAE and PBC in NOD.*c3c4* mice

Female 12-14 wk-old NOD.*c3c4* mice (with established PBC) were immunized with 250 μg of $pMOG_{36-55}$ in CFA s.c. as described above for NOD mice (3). The mice received 350 ng of Pertussis toxin i.v. on days 0 and 2 relative to peptide immunization. Mice were weighed and scored on day 0 and then daily starting on day 14 after immunization, and scores were plotted on a 5-point scale (3). Since these mice, like NOD mice, develop an asynchronous relapsing-remitting form of EAE, all the mice which developed signs of EAE during the first 25 days were randomized into treatment with Cys-NPs or pMHCII-NPs on days 32 or 41 after immunization. All mice were treated twice a week for 6-9 wk. EAE scoring was done as described above. Liver disease scoring involved macroscopic evaluation of cyst content (0-5), liver weight and common bile duct (CBD) diameter (0-4), as well as microscopic evaluation of bile duct involvement (0-4), bile duct proliferation (0-4) and mononuclear cell infiltration (0-4), as described in (5).

Suppression of non-cognate antigen-presentation *in vivo*

Female 8-10-wk-old RIP-DTR-transgenic and non-transgenic NOD mice were treated with DT as described above. DT-treated mice were treated with 10 to 11 doses of $PDC_{166-181}/IA^{g7}$-NPs or Cys-NPs (twice weekly i.v. for 5 weeks). After 9-10 doses, purified splenic 8.3-TCR-transgenic CD8+ T-cells from 8.3-NOD.*G6pc2*$^{-/-}$.*Tcra*$^{-/-}$ donors (using BD IMag anti-mCD8 beads, BD Biosciences) were labeled with 2.5 μM CFSE (Molecular Probes, Eugene, OR), and adoptively transferred i.v. ($5x10^6$ cells/mouse) into DT/pMHCII-NP-treated hosts. After six days, PCLN, PLN and MLN were collected and the cell suspensions stained with anti-mCD8 mAb. Gated CD8+ cells were analyzed for the extent of CFSE dilution using flow cytometry.

IL-10 production capacity

Splenic and liver mononuclear cell suspensions were enriched for CD4+ T-cells using an EasySep™ Mouse CD4 T cells isolation Kit (Stem Cell Technologies). Cells were stained with

pMHCII tetramers and sorted by flow cytometry. The sorted cells ($1–2 \times 10^4$) were stimulated with anti-CD3/CD28 Dynal beads (Dynabeads® Mouse T-Activator CD3/CD28, Thermofisher Scientific) for 3 days at 1:1 cell:cell ratio. Seventy-two hours later, the supernatants were harvested and assayed for IL-10 content via ELISA (Mouse IL-10 DuoSet ELISA, R&D systems).

Histology and serology

Livers were fixed in 10% formalin for 2 days, embedded in paraffin, cut into 5μm sections and stained with H&E or Picrosirius Red. Serum total bile acid (TBA) levels were analyzed using a TBA Enzymatic Cycling Assay Kit (Diazyme, Poway, CA) following a modified manufacturer's protocol as described (10). Alanine aminotransferase (ALT) levels in serum were determined using a kit from Thermo Fisher Scientific following the manufacturer's protocol. Briefly, serum samples were mixed with pre-warmed (37^{o}C) InfinityTM ALT (GPT) Liquid Stable Reagent at 1:10 ratio and OD readings were taken for 3min at 1min intervals in a nanodrop at a 340nm wavelength, 37^{o}C. The slope was calculated by plotting absorbance vs. time using linear regression and multiplied with a factor to obtain ALT levels in serum (U/L) as described in the kit.

Statistical Analysis

Data were compared in GraphPad Prism 6 using Mann-Whitney *U*-test, two-way ANOVA, Log-Rank (Mantel-Cox) or one-way ANOVA with Tukey post-hoc correction. P values <0.05 were considered statistically significant (*P≤0.05; **P<0.01; ***P<0.001; and ****P<0.0001). Sample size given in the legends correspond to the total number of mice studied, pooled from independent experiments.

Supplemental References

1. Hebbandi Nanjundappa R, Ronchi F, Wang J, Clemente-Casares X, Yamanouchi J, Sokke Umeshappa C, et al. A Gut Microbial Mimic that Hijacks Diabetogenic Autoreactivity to Suppress Colitis. *Cell.* 2017;171(3):655-67.
2. Thorel F, Nepote V, Avril I, Kohno K, Desgraz R, Chera S, et al. Conversion of adult pancreatic alpha-cells to beta-cells after extreme beta-cell loss. *Nature.* 2010;464(7292):1149-54.
3. Clemente-Casares X, Blanco J, Ambalavalan P, Yamanouchi J, Singha S, Fandos C, et al. Expanding antigen-specific regulatory networks to treat autoimmunity. *Nature.* 2016;530(7591):434-40.
4. Holdener M, Hintermann E, Bayer M, Rhode A, Rodrigo E, Hintereder G, et al. Breaking tolerance to the natural human liver autoantigen cytochrome P450 2D6 by virus infection. *J Exp Med.* 2008;205(6):1409-22.
5. Umeshappa CS, Singha S, Blanco J, Shao K, Nanjundappa RH, Yamanouchi J, et al. Suppression of a broad spectrum of liver autoimmune pathologies by single peptide-MHC-based nanomedicines. *Nature Comm.* 2019;10(1):2150-2164.
6. Cong Y, Feng T, Fujihashi K, Schoeb TR, and Elson CO. A dominant, coordinated T regulatory cell-IgA response to the intestinal microbiota. *Proc Natl Acad Sci USA.* 2009;106(46):19256-61.
7. Singha S, Shao K, Yang Y, Clemente-Casares X, Sole P, Clemente A, et al. Peptide-MHC-based nanomedicines for autoimmunity function as T-cell receptor microclustering devices. *Nature Nano.* 2017;12(7):701-10.
8. Ishak K, Baptista A, Bianchi L, Callea F, De Groote J, Gudat F, et al. Histological grading and staging of chronic hepatitis. *J Hepatol.* 1995;22(6):696-9.

9. de Vries EM, Verheij J, Hubscher SG, Leeflang MM, Boonstra K, Beuers U, et al. Applicability and prognostic value of histologic scoring systems in primary sclerosing cholangitis. *J Hepatol.* 2015;63(5):1212-9.

10. Bae HR, Leung PS, Tsuneyama K, Valencia JC, Hodge DL, Kim S, et al. Chronic expression of interferon-gamma leads to murine autoimmune cholangitis with a female predominance. *Hepatology.* 2016;64(4):1189-201.

Supplemental Table 1. Autoantigen-specific TR1 cells accumulate in lymph nodes draining sites of autoimmune inflammation in response to both antigen-specific and non-antigen-specific cues but manifestation of their regulatory activity requires local cognate autoantigen expression

Autoimmune Diseases	Beta cell autoantigen-specific Treg cells	CNS autoantigen-specific Treg cells	Ubiquitous autoantigen-specific Treg cells
Pancreatic beta cell autoimmunity	Accumulate in the pancreatic LNs and treat pancreatic autoimmunity (ref. 3)	In the absence of CNS autoimmunity, CNS autoantigen-based pMHC-NPs do not trigger TR1 cell formation/expansion (Ref. 3 and Fig 1C)	Accumulate in the pancreatic LNs in the presence of synchronized massive beta cell loss; Do not accumulate in the liver-draining LNs (Fig. 1C)
Pancreatic beta cell autoimmunity + CNS autoimmunity	Accumulate in the pancreatic LNs; Do not accumulate in the cervical LNs and do not treat CNS autoimmunity (Figs. 1D and 1E-G)	Accumulate in the cervical LNs and treat CNS autoimmunity (Figs. 1D and 1E-G)	Accumulate in the cervical LNs and treat CNS autoimmunity (Figs. 1D and 1E-G)
CNS autoimmunity	In the absence of pancreatic autoimmunity, T1D-relevant pMHC-NPs do not trigger TR1 cell formation/expansion (ref. 3)	Accumulate in the cervical LNs and treat CNS autoimmunity (Figs. 2A, 2B-C)	Accumulate in the cervical LNs and treat CNS autoimmunity; Do not accumulate in the liver-draining LNs (Figs. 2A and 2B-C)
CNS autoimmunity + mild liver autoimmunity (AIH)	In the absence of pancreatic autoimmunity, T1D-relevant pMHC-NPs do not trigger TR1 cell formation/expansion (ref. 3)	Accumulate in the cervical LNs and treat CNS autoimmunity; Do not accumulate in the liver-draining LNs and do not treat liver autoimmunity (Figs. 3A and 3B-F)	Do not accumulate in the cervical LNs or treat CNS autoimmunity; Selectively accumulate in the liver-draining LNs and treat liver autoimmunity (Figs. 3A and 3B-F)
CNS autoimmunity + severe liver autoimmunity (PBC)	In the absence of pancreatic autoimmunity, T1D-relevant pMHC-NPs do not trigger TR1 cell formation/expansion (ref. 3)	Are non-specifically sequestered in the liver-draining LNs without suppressing liver or CNS autoimmunity (Figs. 4A-H)	Selectively accumulate in the liver-draining LNs, suppressing liver but not CNS autoimmunity (Figs. 4A-H)

Supplementary Figure 1

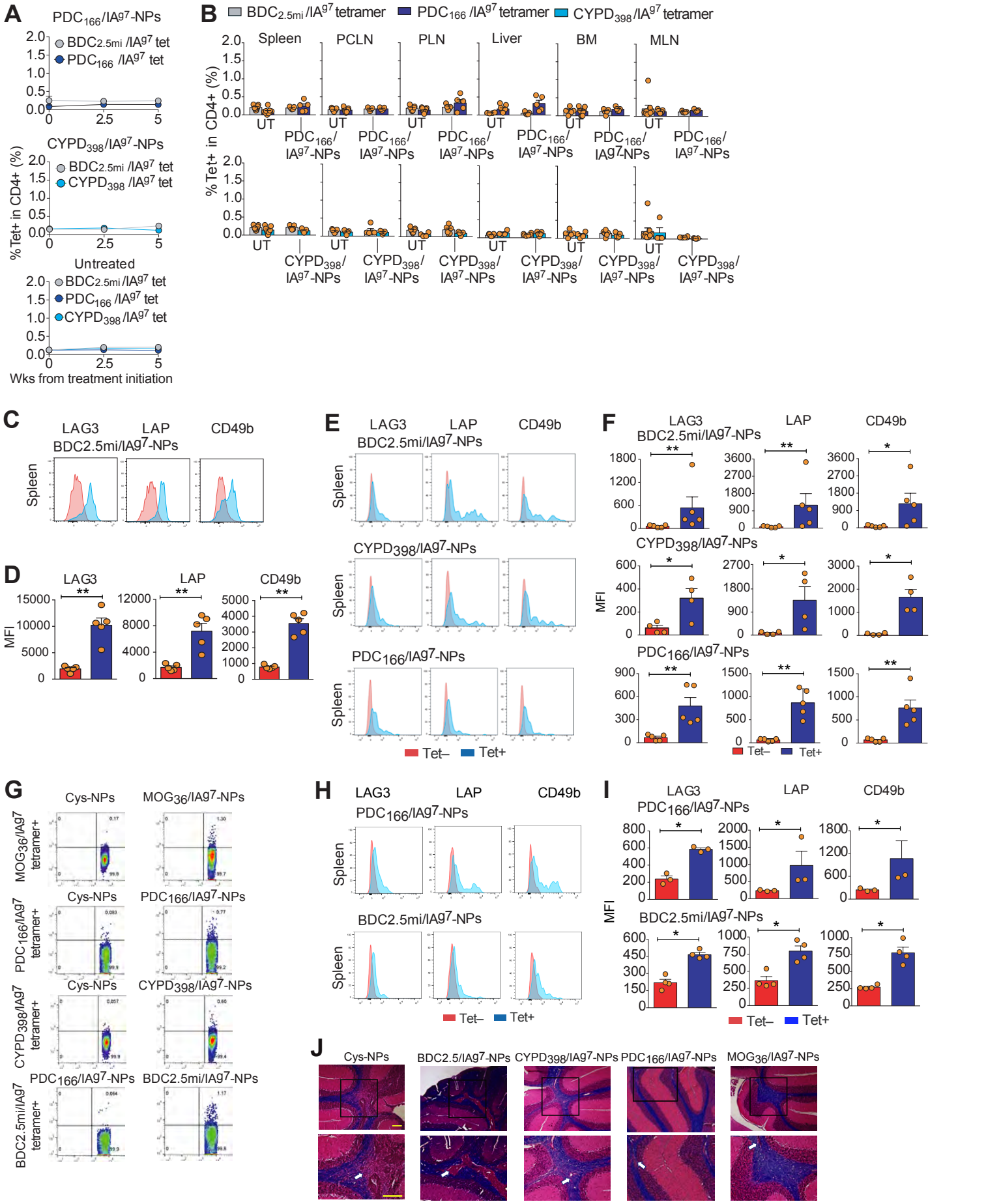

Supplemental Figure 1. Autoantigen shedding renders peripheral autoreactive T-cells responsive to pMHCII-NP therapy and pMHCII-based nanomedicines displaying epitopes from ubiquitous autoantigens blunt relapsing-remitting EAE in NOD mice. A, Percentage of tetramer+CD4+ cells in the blood of pMHCII-NP-treated vs. untreated NOD mice. Data correspond to: (i) 5 $PDC_{166\text{-}181}/IA^{g7}$-NP-treated (2 experiments); (ii) 5 $CYPD_{398\text{-}412}/IA^{g7}$-NP-treated; and (iii) 5 untreated (UT) mice (2 experiments). **B**, Percentages of tetramer+CD4+ cells in NOD mice treated with $PDC_{166\text{-}181}/IA^{g7}$-NPs or $CYPD_{398\text{-}412}/IA^{g7}$-NPs. BM, bone marrow. Data corresponds to 9 untreated, 5 $PDC_{166\text{-}181}/IA^{g7}$-NP-treated (2 experiments each) and 5 $CYPD_{398\text{-}412}/IA^{g7}$-NP-treated mice. **C & D,** Representative histogram plots (**C**) and average mean fluorescence intensity (MFI) values for the TR1 surface markers, LAG3, LAP and CD49b (**D**) on splenic tetramer+ vs. tetramer– cells from BDC2.5mi/IA^{g7}-NP-treated mice (n=5). **E & F**, Representative histogram plots (**E**) and mean fluorescence intensity (MFI) (**F**) for TR1 markers in splenic tetramer+CD4+ cells from 5 $BDC_{2.5mi}/IA^{g7}$-NP-, 5 $PDC_{166\text{-}181}/IA^{g7}$-NP and 4 $CYPD_{398\text{-}412}/IA^{g7}$-NP-treated RIP-DTR-transgenic NOD mice from 2 independent experiments. Data are presented as mean ± SEM. **G**, Representative FACS dot plots of tetramer staining in the spleen of pMHCII-NP-treated NOD mice with EAE. **H & I,** Representative histogram plots (**H**) and MFI (**I**) for TR1 markers in splenic tetramer+CD4+ cells. Data in I correspond to 3 $PDC_{166\text{-}181}/IA^{g7}$-NP- and 4 $BDC_{2.5mi}/IA^{g7}$-NP-treated mice. **J,** Representative luxol fast blue (LFB)/H&E staining pictures of cerebellum from the mice in main Fig. 2B showing inflammation and demyelination (white arrows). Bar = 100μm. Data in D, F and I correspond to the mean ± SEM. P values were calculated using two-way ANOVA (A) or Mann-Whitney U test (B, D, F and I).

Supplementary Figure 2

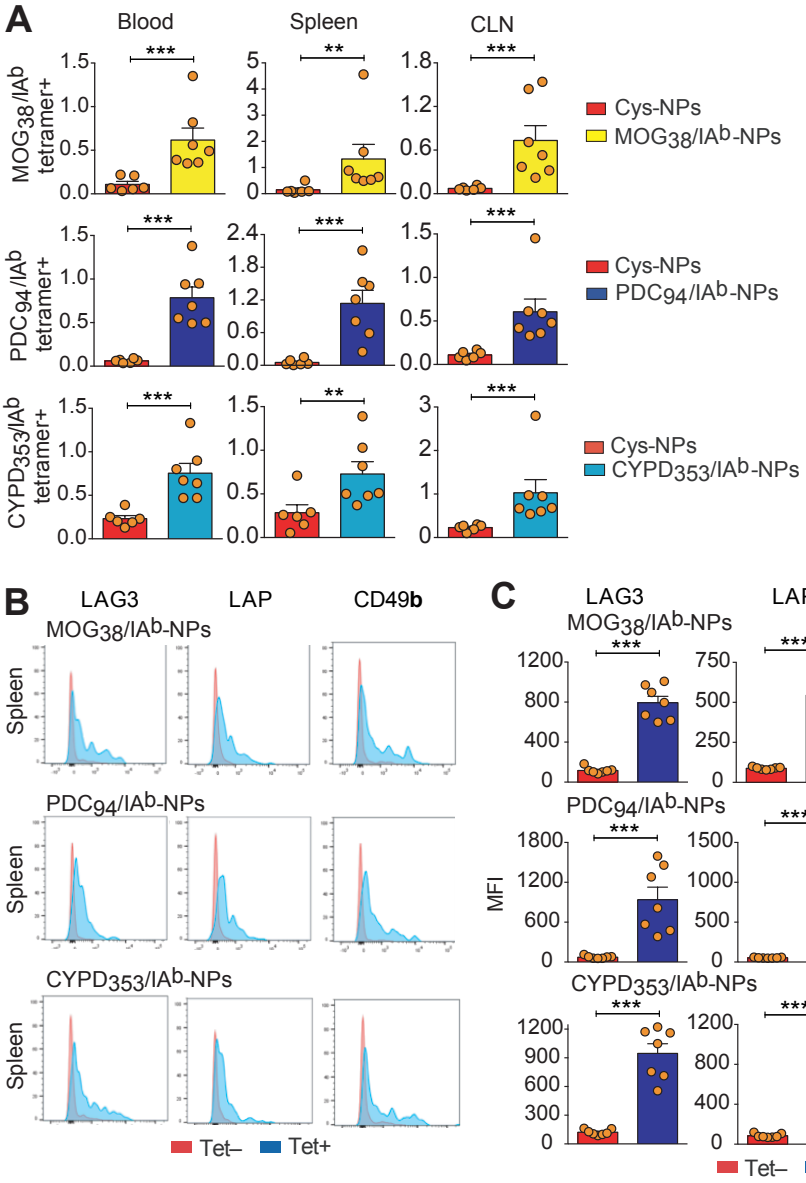

Supplemental Figure 2. TR1 cells recognizing epitopes from ubiquitous autoantigens are recruited to the CNS and blunt chronic progressive EAE in C57BL/6 mice. A, Percentages of tetramer+CD4+ cells in pMHCII-NP-treated C57BL/6J mice with EAE. Data correspond to 6 Cys-NP- and 7 pMHCII-NP-treated mice. **B & C,** Representative histogram plots (**B**) and MFI (**C**) of TR1 markers in splenic tetramer+CD4+ cells. Data correspond to 7 pMHCII-NP-treated mice. Data in A and C correspond to the mean ± SEM. P values were calculated using Mann-Whitney U test.

Supplementary Figure 3

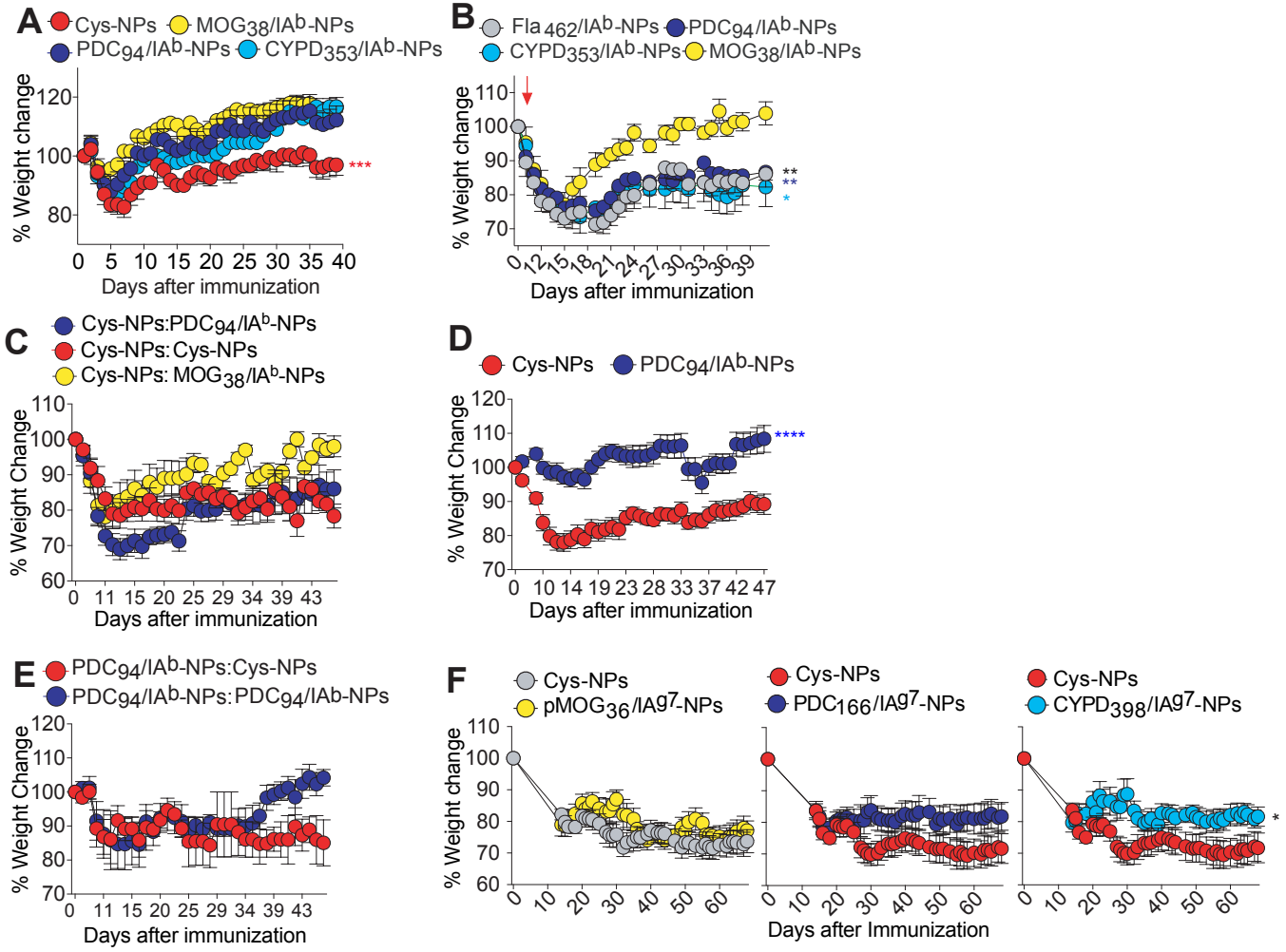

Supplemental Figure 3. Weight loss curves in mice with EAE with and without AIH or PBC upon pMHCII-NP treatment. A, Average weight loss curves for the mice in main Figure 2D. Data correspond to 6 Cys-NP-, 7 MOG_{38-49}/IA^b-NP-, 7 PDC_{94-108}/IA^b-NP- and 7 $CYPD_{353-367}/IA^b$-NP-treated mice. **B**, Average weight loss curves for the mice in main Figure 3A. Data correspond to 11 $Fla_{462-472}/IA^b$-NP-, 7 MOG_{38-49}/IA^b-NP-, 10 PDC_{94-108}/IA^b-NP- and 7 $CYPD_{353-367}/IA^b$-NP-treated mice. **C**, Average weight loss curves for mice in main Figure 3F. Data correspond to n=6 (Cys-NPs), n=7 (PDC-$E2_{94-108}/IA^b$-NPs) and n=7 (MOG_{38-49}/IA^b-NPs) (all received Cys-NPs pre-EAE). **D**, Average weight loss curves for the mice in main Figure 3G (right). Data correspond to n=24 mice/group. **E**, Average weight loss curves for the mice in main Figure 3H. Data correspond to n=3 (Cys-NP) and n=5 (PDC-$E2_{94-108}/IA^b$-NP) (all received PDC-$E2_{94-108}/IA^b$-NPs pre-EAE). **F**, Average weight loss curves for the mice in main Figure 4A. Data correspond to: n=16 mice receiving control NPs (Cys-NP or BDC2.5mi/IA^{g7}-NP) or n=11 mice receiving MOG_{36-50}/IA^{g7}-NPs (left panel); n=11 mice receiving Cys-NP or n=14 mice receiving $PDC_{166-191}/IA^{g7}$-NPs (middle panel); and n=11 mice receiving Cys-NP or n=12 mice receiving $CYPD_{398-412}/IA^{g7}$-NPs (right panel). P values were calculated via two-way ANOVA.

Supplementary Figure 4

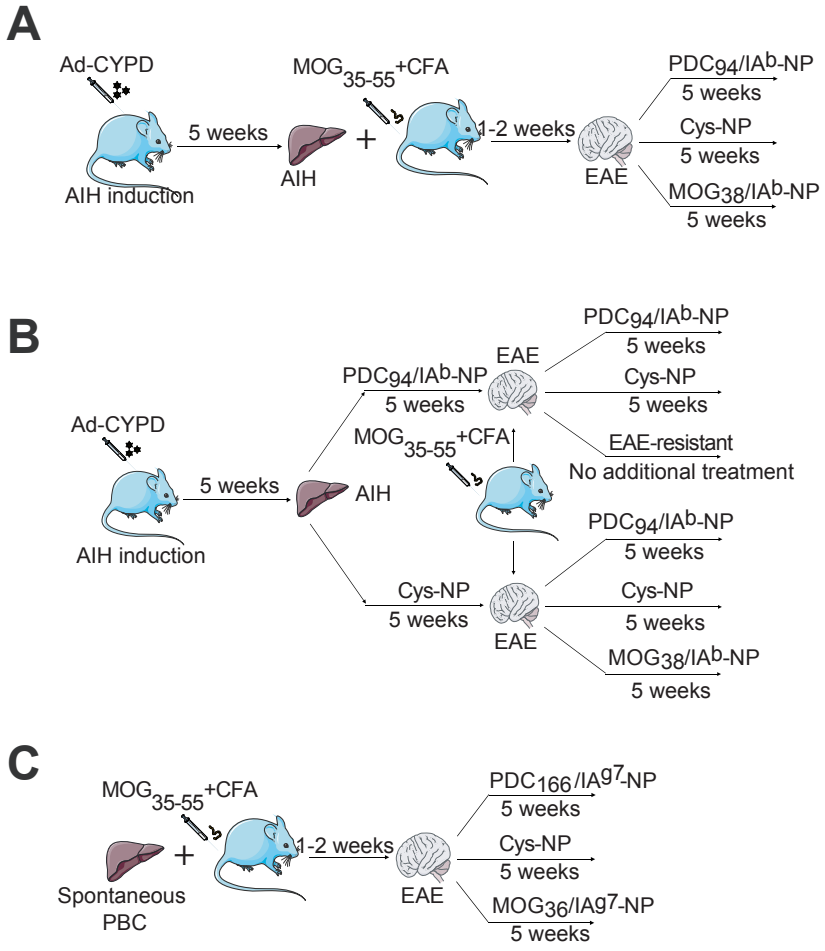

Supplemental Figure 4. Autoimmune disease superimposition flow charts and pMHCII-NP treatment groups. A, Superimposition of EAE onto AIH, followed by treatment with pMHCII-NPs. **B,** Superimposition of EAE onto Cys-NP- or pMHCII-NP-treated AIH, followed by pMHCII-NP treatment. **C**, Superimposition of EAE onto spontaneous PBC, followed by pMHCII treatment.

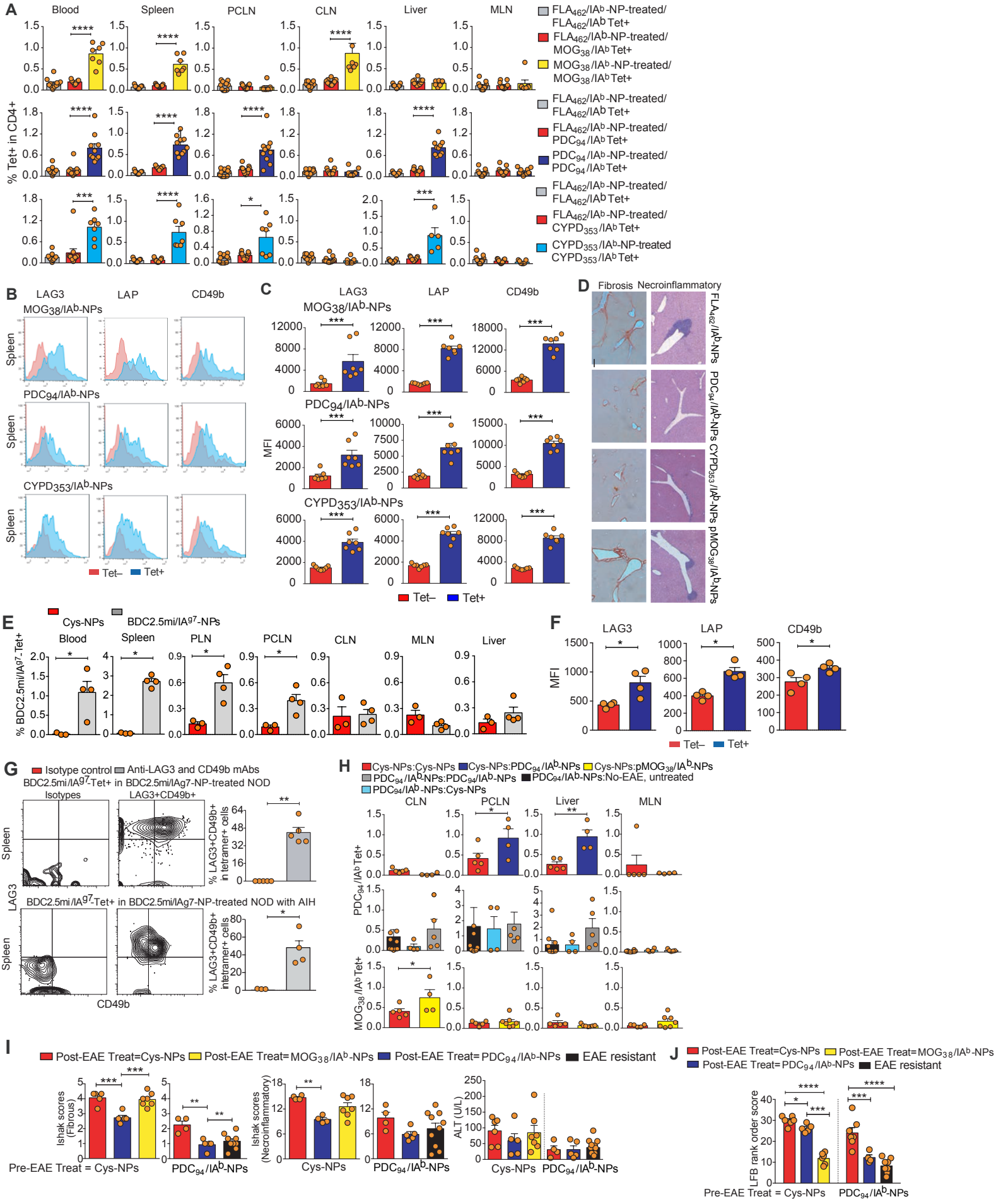
A
Blood
Spleen
PCLN
CLN
Liver
MLN
% Tet+ in CD4+
FLA462/IAb-NP-treated/ FLA462/IAb Tet+
FLA462/IAb-NP-treated/ MOG38/IAb Tet+
MOG38/IAb-NP-treated/ MOG38/IAb Tet+
FLA462/IAb-NP-treated/ FLA462/IAb Tet+
FLA462/IAb-NP-treated/ PDC94/IAb Tet+
PDC94/IAb-NP-treated/ PDC94/IAb Tet+
FLA462/IAb-NP-treated/ FLA462/IAb Tet+
FLA462/IAb-NP-treated/ CYPD353/IAb Tet+
CYPD353/IAb-NP-treated CYPD353/IAb Tet+
B
LAG3
LAP
CD49b
MOG38/IAb-NPs
PDC94/IAb-NPs
CYPD353/IAb-NPs
Spleen
Tet–
Tet+
C
LAG3
LAP
CD49b
MOG38/IAb-NPs
PDC94/IAb-NPs
CYPD353/IAb-NPs
MFI
Tet–
Tet+
D
Fibrosis
Necroinflammatory
FLA462/IAb-NPs
PDC94/IAb-NPs
CYPD353/IAb-NPs
pMOG38/IAb-NPs
E
Cys-NPs
BDC2.5mi/IAg7-NPs
% BDC2.5mi/IAg7-Tet+
Blood
Spleen
PLN
PCLN
CLN
MLN
Liver
F
LAG3
LAP
CD49b
MFI
Tet–
Tet+
G
Isotype control
Anti-LAG3 and CD49b mAbs
BDC2.5mi/IAg7-Tet+ in BDC2.5mi/IAg7-NP-treated NOD
Isotypes
LAG3+CD49b+
Spleen
% LAG3+CD49b+ in tetramer+ cells
BDC2.5mi/IAg7-Tet+ in BDC2.5mi/IAg7-NP-treated NOD with AIH
LAG3
CD49b
H
Cys-NPs:Cys-NPs
Cys-NPs:PDC94/IAb-NPs
Cys-NPs:pMOG38/IAb-NPs
PDC94/IAb-NPs:PDC94/IAb-NPs
PDC94/IAb-NPs:No-EAE, untreated
PDC94/IAb-NPs:Cys-NPs
CLN
PCLN
Liver
MLN
PDC94/IAb Tet+
MOG38/IAb Tet+
I
Post-EAE Treat=Cys-NPs
Post-EAE Treat=MOG38/IAb-NPs
Post-EAE Treat=PDC94/IAb-NPs
EAE resistant
Ishak scores (Fibrous)
Ishak scores (Necroinflammatory)
ALT (U/L)
Pre-EAE Treat = Cys-NPs
PDC94/IAb-NPs
Cys-NPs
J
Post-EAE Treat=Cys-NPs
Post-EAE Treat=MOG38/IAb-NPs
Post-EAE Treat=PDC94/IAb-NPs
EAE resistant
LFB rank order score
Pre-EAE Treat = Cys-NPs
PDC94/IAb-NPs

Supplemental Figure 5. In mice having both EAE and a moderate form of liver inflammation (AIH), ubiquitous antigen-specific TR1 cells, but not their CNS autoantigen-specific counterparts, are selectively recruited to the liver. **A,** Percentages of tetramer+CD4+ cells in C57BL/6J mice having both EAE and AIH, upon pMHCII-NP treatment. Data correspond to: (i) 11 $Fla_{462-472}/IA^{b}$-NP- and 7 MOG_{38-49}/IA^{b}-NP-treated; (ii) 11 $Fla_{462-472}/IA^{b}$-NP- and 10 PDC_{94-108}/IA^{b}-NP-treated; and (iii) 11 $FLA_{462-472}/IA^{b}$-NP- and 7 $CYPD_{353-367}/IA^{b}$-NP-treated. **B & C**, Representative histogram plots (**B**) and MFI (**C**) for TR1 markers in splenic tetramer+CD4+ cells. Data in C correspond to the mean ± SEM values for 7 pMHCII-NP-treated mice in each panel (top to bottom). **D,** Representative H&E- (right) or Picrosirius-Red-stained (left) liver of the mice in main Fig. 3A. Bar = 100μm. **E**, Percentage of tetramer+CD4+ cells in NOD mice with AIH upon treatment with Cys-NPs (n=3) or BDC2.5mi/IA^{g7}-NPs (N=4) for 5 weeks. **F**, Average mean fluorescence intensity values for LAG3, LAP and CD49b for splenic tetramer+ vs. tetramer– cells from BDC2.5mi/IA^{g7}-NP-treated mice with AIH from E (n=4/mAb). **G,** Representative LAG3/CD49b plots and their isotype Ab-stained counterparts for splenic BDC2.5mi/IA^{g7} tetramer+CD4+ T-cells from BDC2.5mi/IAg7-NP-treated NOD mice having (bottom) or not having (top) AIH, along with plots displaying average percentage of double-positive cells (right). Data correspond to n=5 (top) and n=3 (isotypes) and n=4 (specific Abs) (bottom)**. H**, Percentage of tetramer+CD4+ cells in B6 mice having EAE in response to the indicated treatments before and after EAE: top: n=5 and 4; middle, n=10, 4 and 5; bottom: n=5 and 4-7. **I**, Average histopathological scores, and serum ALT levels from the mice in main Figs. 3F and 3H. Data correspond to n=5-6, 5 and 7 (left plot of each readout); and to n= 4, 5 and 10 (right plots)**. J,** Average rank order LFB scores for the mice in H: n=6, 5 and 7 (left); n=7, 4 and 8 (right). Data are represented as the mean ± SEM values and P values were calculated using Mann-Whitney U test (A, C, E and F) or one-way ANOVA with Tukey post-hoc correction (G, H, I and J).

Supplementary Figure 6

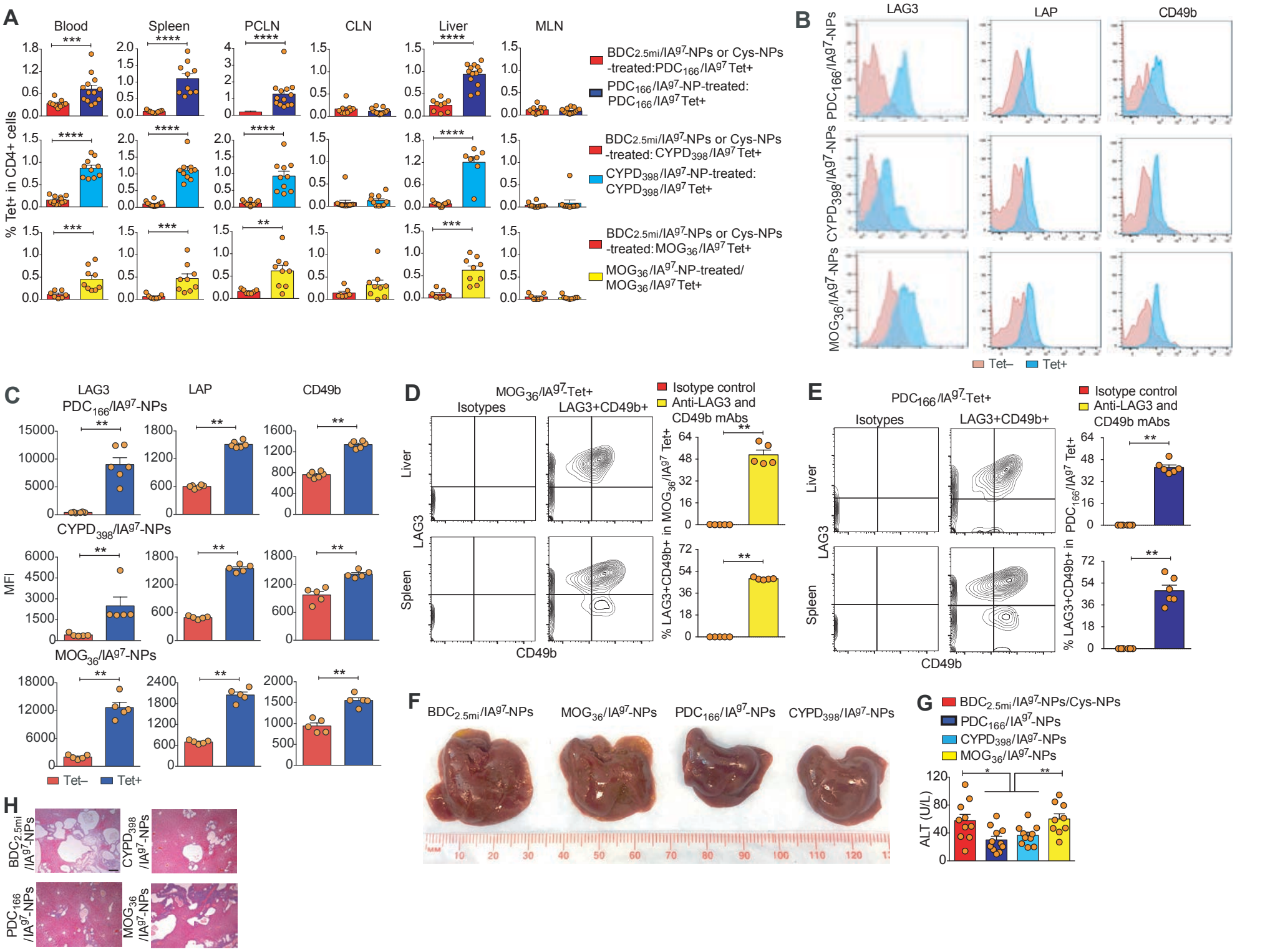

Supplemental Figure 6. In mice having both EAE and a severe form of liver inflammation (PBC), CNS autoantigen-specific TR1 cells are non-specifically sequestered in the liver without suppressing liver disease. A, Percentages of tetramer+CD4+ cells in NOD.*c3c4* mice having both EAE and PBC, upon pMHCII-NP treatment. Data correspond to: n=9 mice receiving control NPs (n=5 Cys-NPs plus n=4 BDC2.5mi/IA^{g7}-NPs) and n=13 mice receiving $PDC_{166\text{-}191}/IA^{g7}$-NPs from 2 experiments (top row); n=12 receiving control NPs (n=8 Cys-NPs plus n=4 BDC2.5mi/IA^{g7}-NPs) and n=8-10 mice receiving $CYPD_{398\text{-}412}/IA^{g7}$-NPs from 2-3 experiments (middle row); and n=7 mice receiving control NPs (n=3 Cys-NPs plus n=4 BDC2.5mi/IA^{g7}-NPs) and n=9 receiving $MOG_{36\text{-}50}/IA^{g7}$-NPs from two experiments (bottom row). **B & C,** Representative histogram plots (**B**) and MFI (**C**) for TR1 markers in splenic tetramer+CD4+ cells. Data in B correspond to 5 to 6 pMHCII-NP-treated mice in each panel. **D-E,** Representative LAG3/CD49b plots and their isotype Ab-stained counterparts for liver and splenic $MOG_{36\text{-}50}/IA^{g7}$ (D) and $PDC_{166\text{-}191}/IA^{g7}$ (E) -tetramer+ CD4+ T-cells (left) along with plots displaying average percentage of double-positive cells (right). Data correspond to n=5 (D) and n=6 (E)**. F,** Representative liver images of mice from main Fig. 4A**. G,** Serum ALT levels in the mice from main Fig. 4A. Data correspond to n=10, 11, 10 and 9 mice/NP type. **H,** Representative H&E liver sections. Bar=100μm. Data are represented as the mean ± SEM. P values were calculated using Mann-Whitney U test (A, C, D and E) or one-way ANOVA with Tukey post-hoc correction (G).